Digital Signal Processing 84 (2019) 59–68

Contents lists available at ScienceDirect

Digital Signal Processing

www.elsevier.com/locate/dsp

A novel multivariate phase synchrony measure: Application to multichannel newborn EEG analysis

Payam Shahsavari Baboukani [a], Ghasem Azemi [a,*], Boualem Boashash [b], Paul Colditz [b], Amir Omidvarnia [c]

[a] Department of Electrical Engineering, Razi University, Kermanshash, Iran
[b] University of Queensland Center for Clinical Research, The University of Queensland, Brisbane, Australia
[c] Florey Institute of Neuroscience and Mental Health and The University of Melbourne, Austin Campus, Melbourne, Australia

ARTICLE INFO

Article history:
Available online 1 October 2018

Keywords:
Multivariate phase synchrony
Circular statistics
Co-integration
S-estimator
Multichannel EEG

ABSTRACT

Phase synchrony assessment across non-stationary multivariate signals is a useful way to characterize the dynamical behavior of their underlying systems. Traditionally, phase synchrony of a multivariate signal has been quantified by first assessing all pair-wise phase relationships between different channels and then, averaging their phase coupling. This approach, however, may not necessarily provide a full picture of multiple phase ratios within non-stationary signals with time-varying statistical properties. Several attempts have been made to generalize pair-wise phase synchrony concept to multivariate signals. In this paper, we introduce a new measure of generalized phase synchrony based on the concept of circular statistics. The performance of the measure is evaluated with simulations using the Kuramoto and Rössler models and compared with that of three existing generalized phase synchrony measures based respectively on 1) the concept of co-integration, 2) S-estimator and 3) hyper-dimensional geometry. The simulation results represent the correct degree of synchronization between channels with negligible mean of squared error, i.e. below $4.2e^{-4}$. We then use the proposed measure to assess inter-hemispheric phase synchrony in two abnormal multichannel newborn EEG datasets with manually marked seizure/non-seizure and burst–suppression signatures. The EEG results suggest that the proposed measure is able to detect inter-hemispheric phase synchrony changes with higher accuracy than the other existing measures, i.e. 2% for seizure/non-seizure database and 11% for burst/suppression database than the best performing existing multivariate phase synchrony measure.

1. Introduction

Phase synchrony analysis is a standard approach for characterizing the dynamics of complex systems with time-varying interactions between their sub-modules. Applications of this approach include detection and modeling of brain dynamics from EEG signals, brain connectivity analysis, and EEG/EEG-fMRI analyses [1–6]. Under such circumstances, quantification of pair-wise phase interactions using bivariate measures such as Phase Locking Value (PLV, also referred to as mean phase coherence or MPC) [7,8], may not be sufficient to outline the global synchrony observed in multivariate dynamics. This challenging problem has led to a new line of research for the evaluation of phase synchrony within multivariate data. The proposed methods include evolution map approach [9], instantaneous period approach [10], mutual prediction approach [10], general field synchronization [11] methods based on Empirical Mode Decomposition (EMD) [12,13], frequency flows analysis [14], phase lag index assessment [15], hyper-dimensional geometry [16], S-estimator measure [17] and generalized phase synchrony (GePS) analysis [1,18].

The multi-layered dynamical structure of the human brain is an example of a complex system with interactive sub-systems, whose activity may be coupled and fluctuate together over time. Understanding the interactions between different cortical areas of the brain is of great importance in medical, cognition and neuroscience applications [19–21]. Such applications include brain abnormality and disorder detection, brain computer interface systems and cognitive load measurement [6,18,22–26]. A non-invasive and common way of investigating such interactions at the scalp level is through multivariate analysis of electroencephalography (EEG) recordings using similarity measures such as coherence, cross correlation and phase synchronization [27–31]. This paper focuses

* Corresponding author.
E-mail address: g.azemi@razi.ac.ir (G. Azemi).

https://doi.org/10.1016/j.dsp.2018.08.019
1051-2004/

on measuring phase synchrony in multivariate signals and applies the proposed methodology to multichannel newborn EEG signals having seizures and burst–suppression (B–S) patterns. Newborn EEG seizure is characterized by variations in amplitude, duration, frequency content and morphology of EEG background [6]. The EEG B–S is characterized by a burst of high voltage activity (75–250 μV), composed of various waveforms, followed by a suppression (<5 μV) [32]. Studies have shown a strong correlation between these abnormal EEG patterns and neurodevelopmental deficits in later stages of childhood [33]. Therefore, automatic detection of these abnormal EEG signatures is of great clinical interest [6,34–36].

Quantification of phase synchrony in non-stationary multivariate signals usually involves two steps: First the instantaneous phase (IP) of each channel is estimated and second, the non-stationary interdependencies between IPs of channels are quantified. The assumption here is that each channel is mono-component, i.e., its time–frequency distribution represents a single time-varying ridge in the time–frequency domain. For multi-component non-stationary signals, therefore, a pre-processing stage is needed in order to decompose them into mono-component signals before IP extraction of each component. This can be done through discrete wavelet transform, empirical mode decomposition, and time–frequency blind source separation [1,21,37,38]. In a multivariate non-stationary signal, the IP of each channel can be extracted using different approaches including complex Gabor wavelet transform and the Hilbert transform with comparable computational cost and performance [39,40]. However, the Hilbert transform-based method offers more simplicity and therefore, is adapted to our analysis framework in this study. Once the IPs have been estimated, the level of phase synchrony among different channels can be quantified. For generalizing bivariate measures to the applications involving K-variate signals, one needs to first calculate phase synchrony of all possible pair-wise couplings ($\frac{K(K-1)}{2}$ comparisons), and then combine them using an integrating operator such as mean (see for example [41]). This approach, however, may not be an efficient representation of multivariate dynamic interactions between channels [42]. In order to address this limitation, techniques such as S-estimator [17], hyper-dimensional geometry [16] and co-integration based GePS [18] have been proposed.

In this paper, we propose an alternative method for quantifying generalized phase synchrony in multivariate signals based on the concept of circular statistics [43]. We then compare its performance with S-estimator method, hyper-dimensional geometry and GePS in a controlled way: we simulate multivariate signals using Kuramoto model and Rössler oscillator [44,45]. We finally show the application of our proposed measure for detection of seizures and B–S patterns in scalp-level newborn EEG signals.

The rest of the paper is organized as follows: Section 2 explains the classical bivariate phase synchrony measures, three existing multivariate synchrony measures as well as the proposed multivariate measure. Section 3 describes the Kuramoto model, Rössler oscillator model and multichannel newborn EEG databases used in this study. Section 4 presents simulations and EEG results. Section 5 discusses the main points, and Section 6 concludes the paper.

2. Methods

In this section, we review the basic concepts behind the existing techniques of bivariate phase synchrony [7,46,47]. This is followed by a review of multivariate phase synchrony approaches including co-integration-based [18], S-estimator method [17] as well as hyper-dimensional geometry approach [16]. Finally, the proposed phase synchrony measure is introduced.

2.1. PLV and the concept of bivariate phase synchrony

In order to extract phase information from a typical real-valued signal, we need to convert it into a complex form. This is commonly done by using the Hilbert transform [48, pp. 31–39]. For a real-valued discrete mono-component signal $x[n]$, the analytic associate $z_x[n]$ is defined as:

$$z_x[n] = x[n] + j\hat{x}[n] = a_x[n]e^{j\phi_x[n]} \tag{1}$$

where $j = \sqrt{-1}$, $\hat{x}[n]$ is the Hilbert transform of $x[n]$, and $a_x[n]$ and $\phi_x[n]$ are the instantaneous amplitude and IP of $x[n]$, respectively. From Eq. (1), the IP signal $\phi_x[n]$ can be obtained as:

$$\phi_x[n] = \tan^{-1}\left(\frac{\hat{x}[n]}{x[n]}\right). \tag{2}$$

If the signal $x[n]$ is multi-component, a preprocessing stage (such as filtering, blind source separation–BSS or EMD) is used to extract the time–frequency components of the signal [1], and then, the IP of each component is estimated separately using (2).

Two signals $x[n]$ and $y[n]$ with N time points and corresponding IPs of $\phi_x[n]$ and $\phi_y[n]$ are called phase locked of order $m:n$ (where m and n are integers) if their IP signals satisfy the following equation [7]:

$$\Delta\phi_{xy}[n] = m\phi_x[n] - n\phi_y[n] = \text{constant}. \tag{3}$$

Several methods have been proposed for measuring phase synchrony in bivariate signals. Most of these methods perform a statistical test to quantify degree of phase locking. For example, methods based on Shannon entropy (e.g., see [46]) quantify the uncertainty of IP differences and mutual information-based methods (e.g., see [47]) measure possible nonlinear relationships between the IPs. For the special case of $m = n = 1$, phase locking between $x[n]$ and $y[n]$ can be quantified by the PLV measure defined as [7]:

$$\eta_{PLV} = \frac{1}{N}\left|\sum_{n=0}^{N-1} e^{j\Delta\phi_{xy}[n]}\right|. \tag{4}$$

The value of η_{PLV} varies between 0 and 1 where 0 means no statistical phase dependency and 1 indicates complete phase synchrony between the two signals.

2.2. Measuring phase synchrony in multivariate signals

In the following, we first review three existing approaches for generalized phase synchrony analysis and then introduce an alternative using the concept of circular statistics.

2.2.1. Co-integration-based phase synchrony measure

Let $\boldsymbol{x}[n] = \{x_1[n], \ldots, x_K[n]\}$ be a K-dimensional signal with the corresponding signal IP $\boldsymbol{\phi_x}[n] = \{\phi_1[n], \ldots, \phi_K[n]\}$. If there are r co-integrating relationships within dimensions of $\boldsymbol{\phi_x}[n]$, the signal $\boldsymbol{x}[n]$ is said to be in generalized phase synchrony of rank r. Here, IP signals are assumed to be integrated signals of order one ($I(1)$), i.e. non-stationary stochastic processes which can be converted into stationary processes by taking the first-order difference [49]. A group of $I(1)$ processes are in a co-integrating relationship of order r, if there are r long-run (i.e., stationary) relations between them. The co-integration rank r is usually estimated using the multivariate Johansen test [49,50]. Based on this concept, a measure for phase synchrony in a given K-dimensional signal can be defined as [18]:

$$\eta_{CI} = \frac{r}{K}. \tag{5}$$

The value of η_{CI} varies between 0 and 1 where $\eta_{CI} = 1$ indicates K stationary relationships between the extracted IPs. More details about the concept of co-integration and the multivariate Johansen test can be found in [49,50].

2.2.2. S-estimator measure

The S-estimator method provides a measure of the level of synchronization across a multivariate dynamical system $\boldsymbol{x}[n]$ using principal components analysis [17]. The assumption here is that the multivariate signal is stationary and each of its channels is a state space variable of the system. Given K channels and N time points for $\boldsymbol{x}[n]$ (i.e., $\boldsymbol{x}[n] = \{x_1[n], \ldots, x_K[n]\},\ n = 1, \ldots, N$), a $K \times K$ matrix is defined as:

$$C_{\boldsymbol{x}} = \frac{1}{N}\boldsymbol{x}^T\boldsymbol{x} \tag{6}$$

where $\boldsymbol{x}^T$ is $\boldsymbol{x}$ transposed. Assuming α_m $(m = 1, 2, \ldots, k)$ is the eigenvalues of the matrix $C_{\boldsymbol{x}}$, the S-estimator η_S is calculated as [17]:

$$\eta_S = 1 + \frac{\sum_{m=1}^{K} \overline{\alpha_m} \log \overline{\alpha_m}}{\log K} \tag{7}$$

where $\overline{\alpha_m} = \frac{\alpha_m}{\sum_{m=1}^{K} \alpha_m}$. Note that η_S varies between 0 and 1, where 1 means perfect synchronization and 0 indicates no dependence within the non-stationary multivariate signal. The rationale behind the S-estimator is that synchronous signals have a more concentrated eigenspectrum and consequently, a lower entropy value (reflected in the right term in Eq. (7)).

2.2.3. Hyper-Torus synchrony

For a K-dimensional signal $\boldsymbol{x}[n] = \{x_1[n], \ldots, x_K[n]\}$ representing the outputs of K oscillators with corresponding IP $\boldsymbol{\phi}_x[n] = \{\phi_1[n], \ldots, \phi_K[n]\}$, consider $\boldsymbol{\varphi}_x[n] = \{\varphi_1[n], \varphi_2[n], \ldots, \varphi_{K-1}[n]\}$ as a $K-1$ angular coordinates; the new quantity $\varphi_i[n]$ shows the difference between $\phi_i[n]$ and circular mean of the phase of the rest of the oscillators, i.e. $\arg(\sum_{\substack{k=1 \\ k\neq i}}^{K} e^{j\phi_k[n]})$ [16]:

$$\varphi_i[n] = \phi_i[n] - \arg\left(\sum_{\substack{k=1 \\ k\neq i}}^{K} e^{j\phi_k[n]}\right). \tag{8}$$

Then direction vectors $\Gamma[n]$ are defined as [16]:

$$\Gamma[n] = \left[\cos(\varphi_1[n]), \sin(\varphi_1[n]), \ldots, \cos(\varphi_K[n]), \sin(\varphi_K[n])\right]; \tag{9}$$

the Hyper-Torus Synchrony (HTS) measure is then defined as:

$$\eta_{HTS} = \frac{1}{N\sqrt{K}} \left\| \sum_{n=1}^{N} \Gamma[n] \right\|_2, \tag{10}$$

where $\|.\|_2$ is the Euclidean norm and N is the number of samples. Note that η_{HTS} also varies between 0 and 1, where 1 means perfect synchronization and 0 indicates no dependence within non-stationary multivariate signal.

2.2.4. The proposed method: circular omega complexity-based phase synchrony measure

The samples of a non-stationary multichannel signal in time form a trajectory in state-space whose dimensionality is an indication of temporal coincidence between the channels [17,51,52]. This observation has led to the introduction of synchrony measures presented in [17]. Similarly, the instantaneous phase information of the signal also represents a trajectory in state-space with a dimensionality affected by the level of phase dependency between channels. Based on this observation, we follow the approach presented in [17] and introduce a new multivariate phase synchrony measure.

Considering the K-dimensional signal $\boldsymbol{x}[n]$ and its corresponding phase signal $\boldsymbol{\phi}_x[n]$ described in Section 2.1, the circular correlation between $\phi_k[n]$ and $\phi_l[n]$ is defined as [43]:

$$c^{\boldsymbol{x}}_{k,l} = \frac{\sum_{n=0}^{N-1} \sin(\phi_k[n] - \overline{\phi}_k) \sin(\phi_l[n] - \overline{\phi}_l)}{\sqrt{\sum_{n=0}^{N-1} \sin^2(\phi_k[n] - \overline{\phi}_k) \sin^2(\phi_l[n] - \overline{\phi}_l)}} \tag{11}$$

where $\overline{\phi}_k$ is the circular mean of $\phi_k[n]$ given by:

$$\overline{\phi}_k = \arg\left(\sum_{n=0}^{N-1} e^{j\phi_k[n]}\right). \tag{12}$$

Now, let us define the circular correlation matrix $CCM^{\boldsymbol{x}} = [c^{\boldsymbol{x}}_{k,l}]_{K\times K}$ with corresponding eigenvalues $\lambda_m;\ m = 1, 2, \ldots, K$. We will show in Section 4.1.1 that in simulated multivariate signals (generated by the Kuramoto model), the eigenvalues of matrix $CCM^{\boldsymbol{x}}$ indicate how synchronized the channels of the signal $\boldsymbol{x}[n]$ are. Specifically, when the channels are synchronized, only the first few eigenvalues will have significant values, whilst the rest will be negligible. On the other hand, when the channels are not synchronized, all K eigenvalues will be uniformly distributed. This can be explained based on the fact that when the channels are not synchronized, dimensionality of their state-space is high and all the eigenvalues are significant, and therefore, are uniformly distributed. On the other hand, when the channels are synchronized, the dimension of their state-space is low and therefore only the first few eigenvalues are significant. Based on the aforementioned facts, we introduce a measure for phase synchrony for multivariate signals. The measure is called circular omega complexity (COC) which quantifies the dimensionality of the state-space (based on IPs) for a K-variate signal and is defined as:

$$\eta_{COC} = 1 + \frac{\sum_{m=1}^{K} \overline{\lambda_m} \log \overline{\lambda_m}}{\log K} \tag{13}$$

where $\overline{\lambda_m} = \frac{\lambda_m}{\sum_{m=1}^{K} \lambda_m}$. Since $\sum_{m=1}^{K} \overline{\lambda_m} = 1$, the basic theorem of information theory [53, pp. 330–380] is met:

$$-\sum_{m=1}^{K} \overline{\lambda_m} \log \overline{\lambda_m} \leq \log K \tag{14}$$

where the equality holds true only when $\overline{\lambda_m} = \frac{1}{K};\ m = 1, 2, \ldots, K$. It follows from (13) and (14) that the η_{COC} varies between 0 and 1 where 0 indicates no phase synchrony between channels of the multichannel signal $\boldsymbol{x}[n]$.

3. Materials for performance evaluation

In this section, multivariate phase synchrony measures introduced in Section 2.2 are evaluated using simulated multivariate signals generated by the Kuramoto model, Rössler oscillator, as well as two datasets of newborn EEG signals with seizure and B–S patterns.

3.1. Simulations

3.1.1. The Kuramoto model

The Kuramoto model provides a mathematical basis for generating coupled oscillators with controlled coupling strength in an analytical manner [45]. It is, therefore, suitable for evaluating the

performance of phase synchrony measures in a controlled way and has found wide applications in neurosciences [54,55].

In the Kuramoto model, the instantaneous frequency of the lth oscillator out of a population of K oscillators is given by:

$$\frac{d\phi_l(t)}{dt} = \omega_l + \frac{k}{K}\sum_{m=1}^{K}\sin\big(\phi_m(t) - \phi_l(t)\big); \quad l = 1, 2, \ldots, K \tag{15}$$

where $\phi_l(t)$ is the instantaneous phase, k is the coupling coefficient, and ω_l is an oscillator-specific natural frequency which follows a Lorentzian distribution given in (16) with mean ω_0 and width β [45]:

$$g(\omega) = \frac{\beta}{\pi[\beta^2 + (\omega - \omega_0)^2]}. \tag{16}$$

The collective phase congruency across the oscillators is quantified by a complex value $R(t)e^{j\psi(t)}$ and defined as [45]:

$$R(t)e^{j\psi(t)} = \frac{1}{K}\sum_{l=1}^{K} e^{j\phi_l(t)}, \tag{17}$$

where $R(t)$ and $\psi(t)$ are the global phase coherence (quantifying phase synchrony among all the oscillators) and average phase, respectively. The phase coherence R is limited to the interval [0 1] and $R = 1$ indicates a perfect synchrony between the oscillators.

3.1.2. Rössler oscillator

The Rössler oscillator can also be used to simulate networks of coupled self-sustained stochastic oscillators with controlled phase synchrony among them [16,44,51]. The system is described as:

$$\begin{cases} \dot{X}_j = -\omega_j Y_j - Z_j + \left[\sum_{i\neq j}\varepsilon_{ij}(X_i - X_j)\right] + \sigma\delta_j \\ \dot{Y}_j = -\omega_j X_j - aY_j \\ \dot{Z}_j = b + (X_j - c)Z_j. \end{cases} \tag{18}$$

In this study, we simulated 6 networks containing 6 oscillators each, using the above equations, (i.e. $i, j = 1, 2, \ldots, 6$). The network configurations are shown in Fig. 1 and have already been used in [16]. Note that Network 1 presents the lowest phase synchronization amongst its oscillators and Network 6 shows the highest.

3.2. Newborn EEG analysis

Two newborn EEG databases were used in this study; both composed of multichannel signals acquired from newborns admitted to the Royal Brisbane and Women's Hospital (RBWH), Brisbane, Australia. The signals were recorded using a Medelec Profile recorder (Medelec, Oxford Instruments, UK) with a monopolar montage and reference to the right or left earlobes according to 10–20 international system of electrode placement. An anti-aliasing low-pass filter with a cutoff frequency of 70 Hz was applied prior to sampling the signals at the rate of 256 Hz.

3.2.1. Seizure database

The EEG seizure database used in this study was comprised of 14-channel signals collected from 10 full-term newborns. In order to enable inter-hemispheric phase synchrony assessment, a symmetrical arrangement of 8 electrodes (F3, F4, C3, C4, P3, P4, O1, O2) were chosen for further analysis. EEG recordings were marked for seizure and non-seizure intervals by a neonatal EEG expert. More details about this database can be found in [56]. Artifact-free 8 second segments (2048 samples) with no overlap were used; 496 seizure segments and 475 non-seizure segments.

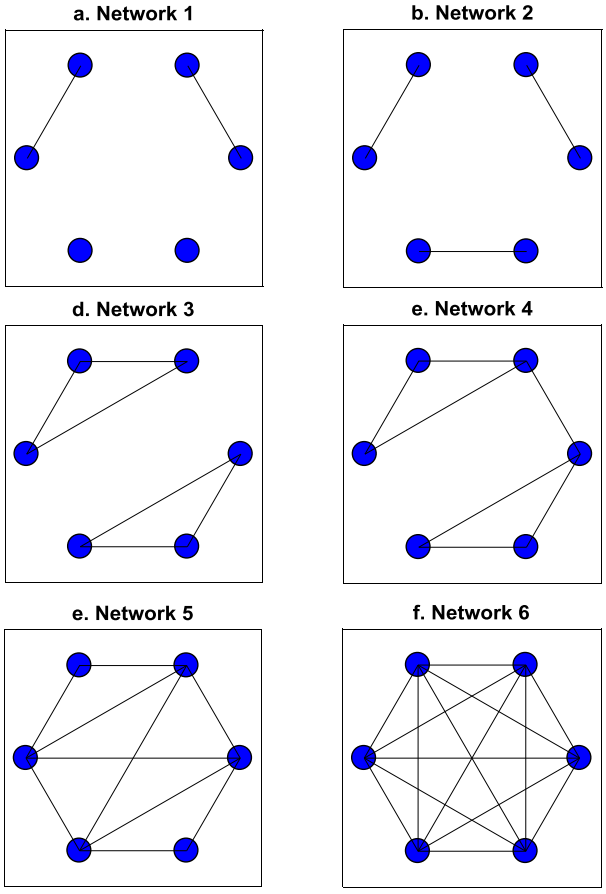

Fig. 1. A set of 6 network configurations used in this paper to study the performance of the phase synchrony measures. (The networks have been presented in an increasing order of generalized phase synchrony.)

3.2.2. Burst–suppression (B–S) database

A 19-channel EEG database was collected from three full-term newborns, born at 38–42 of gestational age. EEG recordings were marked for patterns of burst and suppression intervals by a neonatal EEG expert. Some 115 burst segments with 1 second length and 115 suppression segments with length of 2 seconds were utilized in this study. More details about this database can be found in [36] In order to enable inter-hemispheric phase synchrony assessment, a symmetrical arrangement of 8 electrodes (F3, F4, C3, C4, P3, P4, O1, O2) were chosen for further analysis.

3.2.3. Phase synchrony assessment in multichannel EEG

We performed the analysis steps below for phase synchrony assessment of newborn EEG datasets:

Step 1) Due to the multi-component nature of scalp newborn EEG signals in the time–frequency domain [6], for the EEG seizure database, a band-pass filter was first applied to the signals in the frequency band 1–30 Hz, in which most of the energies of seizure patterns lie. Then, stationary wavelet transform [57] was used to extract the 6th approximate level and the detail levels of 4, 5 and 6. They roughly correspond to the conventional EEG rhythms, namely: δ-band (approximate 6), θ-band (detail 6), α-band (detail 5), β-band (detail 4). For B–S EEG database, a 1–16 Hz band-pass filter was first applied to the signals and then, δ-band (0–4 Hz), θ-band (4–8 Hz) and α-band (8–16 Hz) were extracted using a stationary wavelet transform based approach [57].

Step 2) For each EEG channel at each band, the IP was estimated using the Hilbert transform (see Section 2.1).

Step 3) Multivariate phase synchrony measures were extracted from the resulting multichannel IP within each of the four fre-

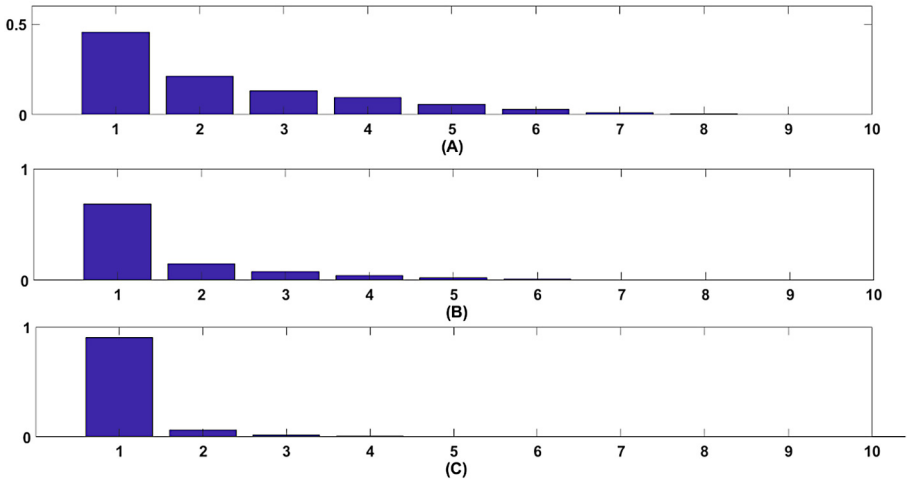

Fig. 2. Distributions of the normalized eigenvalues extracted from the circular correlation matrix of a 10-variate signal generated using the Kuramoto model at 3 different coupling coefficients: A) $k = 0.1$, B) $k = 0.4$, C) $k = 0.7$. As observed, when the oscillators are synchronized, only the first few eigenvalues are significantly higher than 0 and the rest are negligible.

quency bands for the seizure database and three frequency bands for the B–S database.

Step 4) Phase synchrony value (for each measure in Section 2.2) was computed by averaging all band-specific values obtained out of Step 3. The above procedure was repeated for all of the segments. The calculated values were then used to plot the receiver operating characteristic (ROC) curve for each phase synchrony measure. For a given measure, the ROC curve was obtained by plotting its sensitivity against 1-specificity. Sensitivity and specificity are defined as follow [18]:

$$\textit{sensitivity} = \frac{\textit{No of segments correctly marked as seizure or B-S event}}{\textit{No of all seizure or B-S segments}} \tag{19}$$

$$\textit{specificity} = \frac{\textit{No of segments correctly marked as non-seizure or Non B-S event}}{\textit{No of all non-seizure or Non B-S segments}} \tag{20}$$

3.3. Noise analysis

To test the robustness of the proposed phase synchrony measure in the presence of noise, we deliberately added white Gaussian noise to seizure EEG channels, for different values of signal to noise ratio (SNR), ranging from -1 to 10 dB. Noisy EEGs were then analyzed using the proposed phase synchrony measure presented in Section 3.2.3. Finally, for different values of SNR, the area under the resulting ROCs, AUC, were used as the performance measure.

4. Results

4.1. Simulation results

In order to evaluate the performance of the phase synchrony measures, a Kuramoto model with $K = 10$ oscillators was simulated over a time course of 60 seconds. The sampling frequency was chosen to be 50 Hz [42]. The phase synchrony measures defined in Eqs. (5), (7), (10) and (13) (see Section 2.2) were then evaluated using the Monte-Carlo method by averaging over 200 runs. For each run, the natural frequency ω_l was randomly taken from the Lorentzian distribution (defined in Eq. (16)) with initial parameters $\beta = 0.2$ and $\omega_0 = \frac{\pi}{4}$, and the coupling coefficients k was chosen so to ensure that it exceeds its critical value ($k_c = 2\beta$).[1] Coupling coefficient k was varied from 0 to 2 with 0.1 step. The mean values versus the amplitude of the collective phase congruency ($R(t)$) are plotted in Fig. 3.

Table 1
The values of η_{COC} corresponding to the normalized eigenvalue distributions of Fig. 2. As the channels become more synchronized, η_{COC} approaches 1.

Coupling coefficient	0.1	0.4	0.7
η_{COC}	0.37	0.60	0.86

4.1.1. Results of the Kuramoto model

In this section, we show that for a given multivariate signal, the distribution of the eigenvalues of the circular correlation matrix can reveal synchrony between channels of a multivariate signal. For this purpose, the Kuramoto model described in Section 3.1.1 was used to generate a 10-variate signal with 3 different coupling coefficients, 0.1, 0.4, and 0.7. Fig. 2 shows the distributions of normalized eigenvalues extracted from the circular correlation matrix of simulated signals at three coupling coefficients. According to the figure, as the coupling coefficient increases, and the signals become more synchronized, more eigenvalues will tend to negligible values. Specifically, when the coupling coefficient is around 0.7, only the first 3 eigenvalues are significant, and the rest are close to 0. This justifies the use of the entropy of the eigenvalues of the circular correlation matrix as a measure for the phase synchrony in multivariate signals. The corresponding η_{COC} values (given in Table 1) show that as the channels become more synchronized, the COC measure approaches 1.

Fig. 3 shows the performance of phase synchrony measures on the Kuramoto model as a function of its collective phase congruency. Note that we did not use the model for evaluating the S-estimator, as this measure is based on the signals and not their IPs (which the model simulates). As expected, the values of multivariate phase synchrony measures increase as the coupling coefficient increases. All measures exhibit negligible errors when the channels are in complete synchronization. However, for small values of the coupling coefficient, the co-integration-based measure shows lower performance. It is seen that the COC-based measure exhibits

[1] Synchronization amongst the oscillators does not increase with increasing k when k exceeds its critical value.

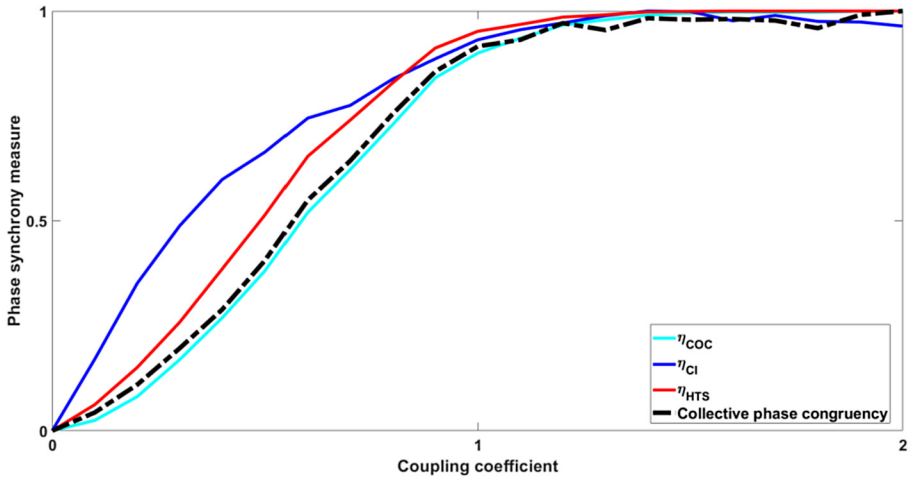

Fig. 3. The normalized values of the three multivariate phase synchrony measures for a simulated 10-variate signal with different coupling coefficients. Also shown is the average coherence of the output of the Kuramoto which can be considered the gold standard. The proposed η_{COC} follows the pattern most similar to the average coherence with negligible bias. (For interpretation of the colors in the figure(s), the reader is referred to the web version of this article.)

a similar pattern to the average coherence with negligible bias and outperforms the other measure.

Then, the mean square error (MSE) between the values of the multivariate phase synchrony measures and the average coherence was computed in order to shows how close the estimated phase synchrony value is close to the real value, i.e. the gold standard (the black curve). For each value of the coupling coefficient, the error for each phase synchrony measure is found by subtracting the value of the measure from the gold standard value. The mean of the squared errors is used as a criterion. Note that all the 3 measures are normalized between 0 and 1. The resulting MSE is dimensionless similarly to the values of phase synchrony measures. The MSE value of the COC-based is $4.2e^{-4}$ which is significantly lower than that of the co-integration based measure that is 0.0186 and HTS which is 0.003.

4.1.2. Rössler model results

In order to check the performance of the proposed measure in networks of oscillators formed by nonlinear systems in a chaotic regime, the Rössler model with 6 oscillators according to (18) with different configurations was also simulated, as shown in Fig. 1. The model parameters are as follows: $a = 0.35$, $b = 0.2$, $c = 10$, $\omega_1 = 1.05$, $\omega_2 = 1.03$, $\omega_3 = 1.01$, $\omega_4 = 0.99$, $\omega_5 = 0.97$, $\omega_6 = 0.95$, $\sigma = 1.5$. The parameter δ_j was considered as a normal distributed random number with unit variance, and ε_{ij} determines the coupling between the ith and jth oscillators. In this work, $\varepsilon_{ij} = \varepsilon_{ji} = 0.5$ was chosen for coupled oscillators and $\varepsilon_{ij} = 0$ for the non-coupled ones. The sampling frequency was 50 Hz and the signals were simulated over a time span of 60 seconds. The phase synchrony measures of Section 2.2 were extracted from the 6 networks presented in Fig. 1. The calculated values are given in Table 2. The results show that all phase synchrony measures successfully detect the increase in the multivariate phase synchrony amongst the oscillators in the networks, except η_{CI} for networks 5 and 6. As Table 2 suggests, the phase synchrony value of the proposed measure for network 6 which is completely synchronous, should be 1; it is lower than the rest of measures, specially HTS and S-estimator measures but it shows better results in network 1 and 2, i.e. phase synchrony values for these networks should be significantly lower than the rest of networks. For example, the proposed measure value of the network 1 is 0.20 which is considerably lower than that of network 6 (0.90) while the values for HTS measure, for example, are 0.72 and 0.99. However, the results suggest that the proposed measure exhibits higher sensitivity than the other ones.

Table 2
Multivariate synchrony values for six networks produced by Rössler oscillator model.

Network	η_{COC}	η_{CI}	η_S	η_{HTS}
1	0.20 ± 0.05	0.81 ± 0.13	0.58 ± 0.04	0.72 ± 0.06
2	0.25 ± 0.04	0.82 ± 0.16	0.74 ± 0.06	0.84 ± 0.06
3	0.46 ± 0.05	0.88 ± 0.14	0.84 ± 0.04	0.90 ± 0.05
4	0.64 ± 0.10	0.94 ± 0.09	0.94 ± 0.01	0.97 ± 0.008
5	0.80 ± 0.05	0.91 ± 0.1	0.97 ± 0.006	0.98 ± 0.003
6	0.90 ± 0.01	0.89 ± 0.13	0.98 ± 0.002	0.99 ± 0.001

4.2. Newborn EEG results

The ROC curves obtained from the analysis of seizure/non-seizure segments and B–S segments using the four generalized phase synchrony measures are shown in Fig. 4A and B, respectively. AUC values summarized in Tables 3 and 4 indicate that EEG channels are more synchronized during seizure periods than non-seizure periods and more synchronized during burst segments than suppression segments. They also suggest that among the four multivariate phase synchrony measures, η_{COC}, attains the maximum AUC and thus best detects the phase synchrony among the EEG channels.

Next, a two-sample t-test was applied to the phase synchrony measures calculated for all seizure (burst) and non-seizure (suppression) segments. In all cases, the values calculated from seizure (burst) segments had a higher mean than the non-seizure (suppression) segments. Therefore, the null hypothesis of equal means between the two groups was rejected (p-values reported in Tables 3 and 4). Among the four multivariate synchrony measures considered, η_{COC} performs best.

4.3. Noise analysis results

Noise analysis results are summarized in Fig. 5. It is observed that all phase synchrony measures for all values of SNR are significantly different from the chance level (AUC = 50%). However, again η_{COC} has a better performance than the others at all SNRs. As Fig. 5 shows, the AUC values obtained from η_{COC} vary between 0.77 and 0.86 in contrast to η_{HTS} (varying between 0.73 and 0.80), η_S (varying between 0.56 and 0.80) and η_{CI} (varying between 0.52 and 0.61).

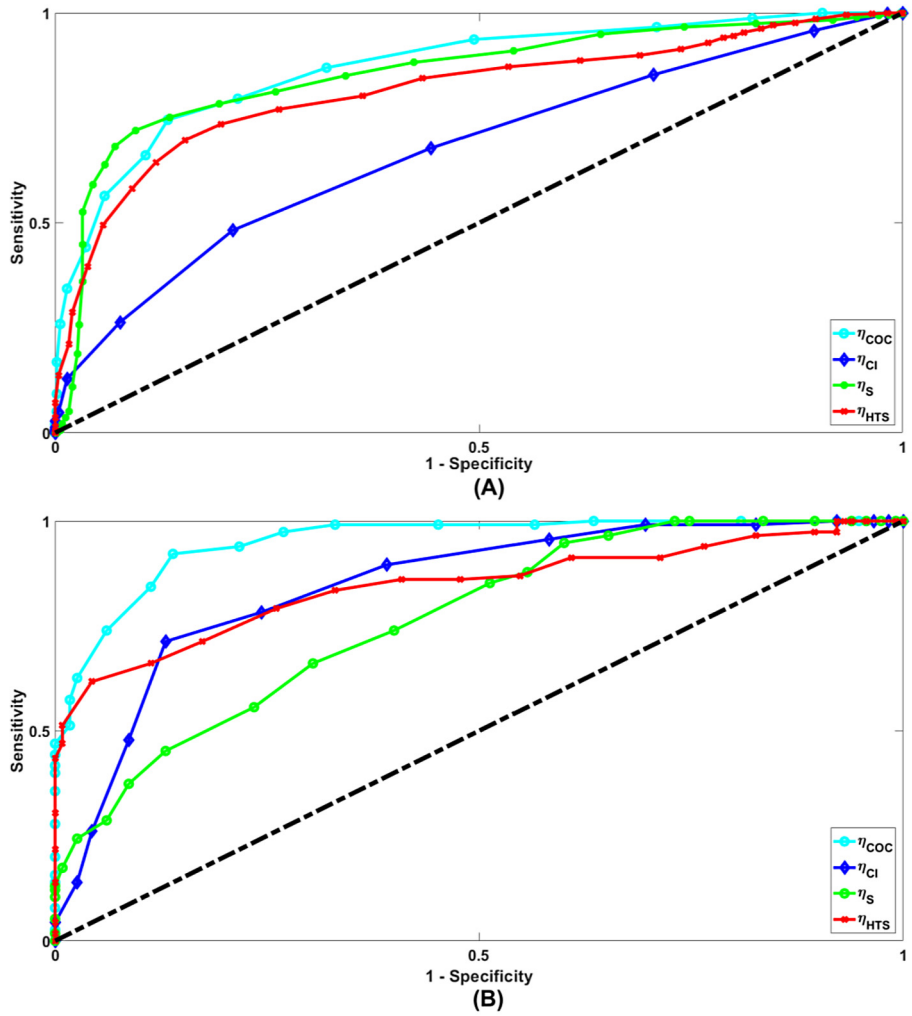

Fig. 4. ROC curves of the phase synchrony methods in this study: A) within seizure and non-seizure EEG segments, B) within burst and suppression EEG segments.

Table 3
AUC values associated with Fig. 4A along with the p-values of the t-test and Mean ± SD of each measure.

Measure	η_{COC}	η_{CI}	η_S	η_{HTS}
AUC	87.13	67.35	85.77	81.61
p-Value	<0.001	<0.001	<0.001	<0.001
Mean ± SD of seizure segments	0.21 ± 0.07	0.13 ± 0.06	0.55 ± 0.11	58.11 ± 0.11
Mean ± SD of non-seizure segments	0.10 ± 0.05	0.10 ± 0.04	0.38 ± 0.09	0.43 ± 0.12

Table 4
AUC values associated with Fig. 4B along with p-values of the t-test and Mean ± SD of each measure.

Measure	η_{COC}	η_{CI}	η_S	η_{HTS}
AUC	95.16	84.65	76.63	84.52
p-Value	<0.001	<0.001	<0.001	<0.001
Mean ± SD of burst segments	0.54 ± 0.11	0.67 ± 0.08	0.77 ± 0.08	0.80 ± 0.1
Mean ± SD of suppression segments	0.32 ± 0.07	0.53±0.1	0.67 ± 0.09	0.65 ± 0.09

5. Discussion

The use of bivariate phase synchrony measures to applications involving multivariate signals requires pair-wise phase synchrony assessment between different channels and then combining the bivariate phase synchrony values. This process can be very time-consuming and computationally expensive, especially when the number of channels is high. Even so, the final result may not necessarily provide a full picture of global interactions in non-stationary signals with time-varying statistical properties. For such applications, this paper takes the concept of 'generalized phase synchrony' further by introducing a new phase synchrony measure for multivariate signals. In contrast to the co-integration based measure that is based on MVAR modeling of the underlying signals [18,49], the proposed measure is model-free and needs no parameter estimation. This is of particular importance for real-world signals with inherent non-stationarity and time-varying statistical properties such as electroencephalogram (EEG) recordings.

The performance analysis of the multivariate phase synchrony measures, using simulated multivariate signals generated by the Kuramoto model, showed that the proposed measure exhibits the most similar pattern to the global phase coherence of the model, i.e. lowest MSE value in comparison with existing measures. Also, the simulation results using Rössler model demonstrate that the proposed measure is more sensitive to changes in the synchronization amongst oscillators in the network. This feature can be very

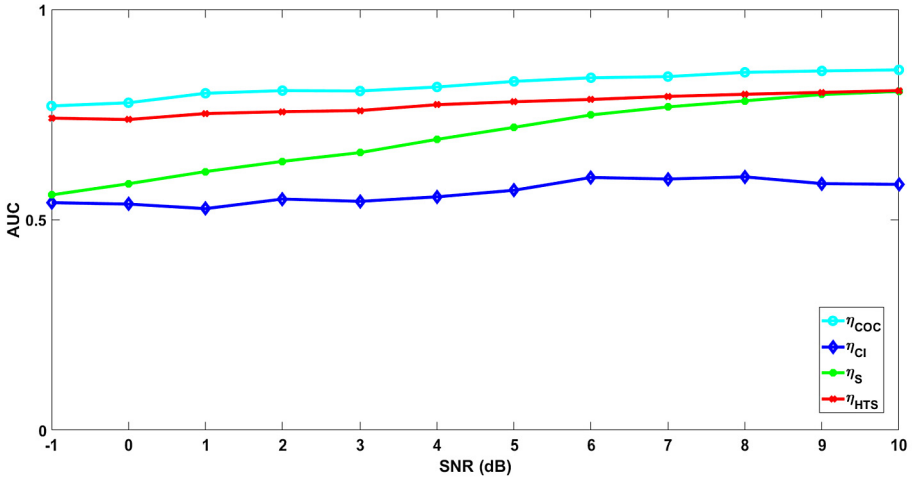

Fig. 5. AUC values associated with different SNR levels for the four synchrony measures.

useful, for example, for estimating the cognitive work load using EEG where small changes in the work load results in negligible change in the synchronization between EEG channels [26].

The proposed measure was then used to discriminate between seizure/non-seizure and burst/suppression segments of real newborn multichannel EEG recordings. Due to the multicomponent nature of such signals, the components were first extracted and, at the final stage, following the approach presented in [6,18], multivariate phase synchrony values calculated for different components were combined using the mean operator. From a signal processing point of view, the final value shows how much all different components in the signals are synchronized. In some other applications, e.g. EEG monitoring for cognitive load assessment [58], combining band-specific markers using other statistics like maximum or median may result in more accurate measurement of phase synchrony between the channels.

The proposed measure was compared with the S-estimator based measure, and the obtained results demonstrate that the proposed measure outperform the other measure. Better results may be caused by the fact that phase synchrony measures provide amplitude-free connectivity between cortical regions, and so are less susceptible to the effects of artifact, inter-trial and inter-subject amplitude variability than cross-correlation, coherence and S-estimator which are depended on amplitude of the signal [21, 59]. The experimental results showed that the proposed measure achieves the highest AUC, for both EEG seizure/non-seizure and EEG burst/suppression databases. Specifically, for seizure/non-seizure database, the AUC of the proposed method was 87.13% in comparison with 67.35%, 85.77% and 81.61% for co-integration based, S-estimator and HTS methods, respectively. And, for the B–S database, the proposed method achieved the AUC of 95.16%, almost 11% better than the best performing existing method. The results show that the level of phase synchrony is elevated during seizure intervals. This observation of increasing inter-hemispheric phase synchrony across scalp EEG channels during seizure periods is consistent with previous studies [18]. Also, the level of inter-hemispheric synchrony across EEG during burst segments was found to be significantly higher than suppression segments. Tables 2 and 3 show the results of two sample t-tests applied to the values of the phase synchrony measures calculated for all seizure (burst) and non-seizure (suppression) segments; these results are completely consistent with the results of the ROC analysis and both analyses confirm a statistical difference between seizure (burst) and non-seizure (suppression) segments and show significantly higher inter-hemispheric connectivity during seizure (burst) periods compared to non-seizure (suppression) periods. The analysis of real multichannel EEGs in the presence of AWGN showed that the proposed phase synchrony measure is robust to noise; a feature which is of great importance in application were the signals are affected by noise, artifacts and interference.

6. Conclusion

In this paper, we introduced a new measure based on circular statistics for quantifying the generalized phase synchrony (GePS) in multivariate signals. In order to evaluate the performance of the proposed measure and compare it with that of existing multivariate measures in a controlled way, we simulated multivariate signals using the Kuramoto and Rössler models. We have deliberately used single-dimension dynamic models in our simulation analyses in order to characterize the most basic aspects of generalized phase synchrony measures. Quantification of phase synchrony in a network of chaotic oscillators formed by connecting different nonlinear systems in chaotic regimes (e.g., Lorenz and Rössler systems) or in real-world systems (e.g., the human brain) deserves an independent and comprehensive study and will be considered in future work.

The methodology presented in this paper used the Hilbert transform to estimate instantaneous phases of the signals. Other methods such as continuous wavelet transform can also be used [39]. We then investigated the applicability of the proposed measure for inter-hemispheric phase synchrony assessment of multichannel newborn EEG. For the analysis of multichannel newborn EEGs, this study used the stationary wavelet transform (SWT) to decompose the signals. Other techniques such as band-pass filtering, empirical mode decomposition (EMD) and blind source separation can also be used for decomposing signals. Designing an optimum methodology for the analysis of such signals requires finding the best decomposition technique which results in more accurate estimation of phase synchrony among channels. The achieved results show that the proposed measure is able to quantify multivariate phase synchrony in simulated and real multivariate signals with less bias compared to existing multivariate phase synchrony measures. This should result in accuracy improvements in a wide range of applications such as brain modeling [3,5], brain connectivity analysis [6,60], EEG abnormality detection [6,18], simultaneous EEG-fMRI analysis [61,62], and EEG-based brain computer interfaces [63]. Despite its good performance for simulated and real multivariate signals, the main limitation of the proposed measure is that it still depends on bivariate values. In order to overcome this limitation, the authors plan to develop a multivariate phase

synchrony based on the concept of mutual information in future work.

Acknowledgments

The newborn data used in this paper were collected in UQCCR as part of three Qatar Foundation NPRP grants (NPRP 4-1303-2-517, NPRP 9-465-2-174 and NPRP 6-885-2-364 awarded to Profs. B. Boashash and P. Colditz).

References

[1] B. Boashash, A. Aïssa-El-Bey, Robust multisensor time–frequency signal processing: a tutorial review with illustrations of performance enhancement in selected application areas, Digit. Signal Process. 77 (2018) 153–186.
[2] A.G. Mahyari, D.M. Zoltowski, E.M. Bernat, S. Aviyente, A tensor decomposition-based approach for detecting dynamic network states from EEG, IEEE Trans. Biomed. Eng. 64 (2017) 225–237.
[3] K. Mahjoory, W. Nikulin, L. Botrel, K. Linkenkaer-Hansen, M.M. Fato, S. Haufe, Consistency of EEG source localization and connectivity estimates, Neuroimage 152 (2017) 590–601.
[4] A. Omidvarnia, M. Pedersen, J.M. Walz, D.N. Vaughan, D.F. Abbott, G.D. Jackson, Dynamic regional phase synchrony (DRePS), Hum. Brain Mapp. 37 (2016) 1970–1985.
[5] M. Rubinov, O. Sporns, Complex network measures of brain connectivity: uses and interpretations, NeuroImage 52 (2010) 1059–1069.
[6] B. Boashash, G. Azemi, J.M. O'Toole, Time–frequency processing of nonstationary signals: advanced TFD design to aid diagnosis with highlights from medical applications, IEEE Signal Process. Mag. 30 (2013) 108–119.
[7] J.-P. Lachaux, E. Rodriguez, J. Martinerie, F.J. Varela, Measuring phase synchrony in brain signals, Hum. Brain Mapp. 8 (1999) 194–208.
[8] F. Mormann, K. Lehnertz, P. David, C.E. Elger, Mean phase coherence as a measure for phase synchronization and its application to the EEG of epilepsy patients, Physica D, Nonlinear Phenom. 144 (2000) 358–369.
[9] M.G. Rosenblum, A.S. Pikovsky, Detecting direction of coupling in interacting oscillators, Phys. Rev. E 64 (2001) 045202.
[10] M.G. Rosenblum, L. Cimponeriu, A. Bezerianos, A. Patzak, R. Mrowka, Identification of coupling direction: application to cardiorespiratory interaction, Phys. Rev. E 65 (2002) 041909.
[11] T. Koenig, D. Lehmann, N. Saito, T. Kuginuki, T. Kinoshita, M. Koukkou, Decreased functional connectivity of EEG theta-frequency activity in first-episode, neuroleptic-naıve patients with schizophrenia: preliminary results, Schizophr. Res. 50 (2001) 55–60.
[12] D. Looney, C. Park, P. Kidmose, M. Ungstrup, D. Mandic, Measuring phase synchrony using complex extensions of EMD, in: 2009 IEEE/SP 15th Workshop on Statistical Signal Processing, 2009, pp. 49–52.
[13] A.Y. Mutlu, S. Aviyente, Multivariate empirical mode decomposition for quantifying multivariate phase synchronization, EURASIP J. Adv. Signal Process. 2011 (2011) 1–13.
[14] D. Rudrauf, A. Douiri, C. Kovach, J.-P. Lachaux, D. Cosmelli, M. Chavez, C. Adam, B. Renault, J. Martinerie, M. Le Van Quyen, Frequency flows and the time–frequency dynamics of multivariate phase synchronization in brain signals, NeuroImage 31 (2006) 209–227.
[15] C.J. Stam, G. Nolte, A. Daffertshofer, Phase lag index: assessment of functional connectivity from multi channel EEG and MEG with diminished bias from common sources, Hum. Brain Mapp. 28 (2007) 1178–1193.
[16] M. Al-Khassaweneh, M. Villafañe-Delgado, A.Y. Mutlu, S. Aviyente, A measure of multivariate phase synchrony using hyperdimensional geometry, IEEE Trans. Signal Process. 64 (2016) 2774–2787.
[17] K. Oshima, C. Carmeli, M. Hasler, State change detection using multivariate synchronization measure from physiological signals, J. Signal Process. 10 (2006) 223–226.
[18] A. Omidvarnia, G. Azemi, P.B. Colditz, B. Boashash, A time–frequency based approach for generalized phase synchrony assessment in nonstationary multivariate signals, Digit. Signal Process. 23 (2013) 780–790.
[19] K. Ansari-Asl, J.-J. Bellanger, F. Bartolomei, F. Wendling, L. Senhadji, Time–frequency characterization of interdependencies in nonstationary signals: application to epileptic EEG, IEEE Trans. Biomed. Eng. 52 (2005) 1218–1226.
[20] F. Bartolomei, I. Bosma, M. Klein, J.C. Baayen, J.C. Reijneveld, T.J. Postma, J.J. Heimans, B.W. van Dijk, J.C. de Munck, A. de Jongh, Disturbed functional connectivity in brain tumour patients: evaluation by graph analysis of synchronization matrices, Clin. Neurophysiol. 117 (2006) 2039–2049.
[21] I. Daly, S.J. Nasuto, K. Warwick, Brain computer interface control via functional connectivity dynamics, Pattern Recognit. 45 (2012) 2123–2136.
[22] E. Gysels, P. Celka, Phase synchronization for the recognition of mental tasks in a brain–computer interface, IEEE Trans. Neural Syst. Rehabil. Eng. 12 (2004) 406–415.
[23] M.G. Knyazeva, C. Carmeli, A. Khadivi, J. Ghika, R. Meuli, R.S. Frackowiak, Evolution of source EEG synchronization in early Alzheimer's disease, Neurobiol. Aging 34 (2013) 694–705.
[24] A. Omidvarnia, G. Azemi, B. Boashash, J.M. O'Toole, P.B. Colditz, S. Vanhatalo, Measuring time-varying information flow in scalp EEG signals: orthogonalized partial directed coherence, IEEE Trans. Biomed. Eng. 61 (2014) 680–693.
[25] T. Sobayo, A.S. Fine, E. Gunnar, C. Kazlauskas, D. Nicholls, D.J. Mogul, Synchrony dynamics across brain structures in limbic epilepsy vary between initiation and termination phases of seizures, IEEE Trans. Biomed. Eng. 60 (2013) 821–829.
[26] P. Zarjam, J. Epps, F. Chen, N.H. Lovell, Estimating cognitive workload using wavelet entropy-based features during an arithmetic task, Comput. Biol. Med. 43 (2013) 2186–2195.
[27] L. Astolfi, F. De Vico Fallani, F. Cincotti, D. Mattia, M. Marciani, S. Salinari, J. Sweeney, G. Miller, B. He, F. Babiloni, Estimation of effective and functional cortical connectivity from neuroelectric and hemodynamic recordings, IEEE Trans. Neural Syst. Rehabil. Eng. 7 (2009) 224–233.
[28] R. Guevara, J.L.P. Velazquez, V. Nenadovic, R. Wennberg, G. Senjanović, L.G. Dominguez, Phase synchronization measurements using electroencephalographic recordings, Neuroinformatics 3 (2005) 301–313.
[29] R.Q. Quiroga, A. Kraskov, T. Kreuz, P. Grassberger, Performance of different synchronization measures in real data: a case study on electroencephalographic signals, Phys. Rev. E 65 (2002) 041903.
[30] C. Rummel, E. Abela, M. Müller, M. Hauf, O. Scheidegger, R. Wiest, K. Schindler, Uniform approach to linear and nonlinear interrelation patterns in multivariate time series, Phys. Rev. E 83 (2011) 066215.
[31] V. Sakkalis, C.D. Giurcaneanu, P. Xanthopoulos, M.E. Zervakis, V. Tsiaras, Y. Yang, E. Karakonstantaki, S. Micheloyannis, Assessment of linear and nonlinear synchronization measures for analyzing EEG in a mild epileptic paradigm, IEEE Trans. Inf. Technol. Biomed. 13 (2009) 433–441.
[32] J.J. Volpe, Neurology of the Newborn, Elsevier Health Sciences, vol. 899, 2008.
[33] M.A. Awal, M.M. Lai, G. Azemi, B. Boashash, P.B. Colditz, EEG background features that predict outcome in term neonates with hypoxic ischaemic encephalopathy: a structured review, Clin. Neurophysiol. 127 (2016) 285–296.
[34] B. Boashash, G. Azemi, N.A. Khan, Principles of time–frequency feature extraction for change detection in non-stationary signals: applications to newborn EEG abnormality detection, Pattern Recognit. 48 (2015) 616–627.
[35] B. Boashash, S. Ouelha, Automatic signal abnormality detection using time–frequency features and machine learning: a newborn EEG seizure case study, Knowl.-Based Syst. 106 (2016) 38–50.
[36] P. Mirzaei, G. Azemi, N. Japaridze, B. Boashash, Surrogate data test for nonlinearity of EEG signals: a newborn EEG burst suppression case study, Digit. Signal Process. 70 (2017) 30–38.
[37] J. Lerga, V. Sucic, B. Boashash, An efficient algorithm for instantaneous frequency estimation of nonstationary multicomponent signals in low SNR, EURASIP J. Adv. Signal Process. 2011 (2011) 1–16.
[38] J. Zhang, N. Wang, H. Kuang, R. Wang, An improved method to calculate phase locking value based on Hilbert–Huang transform and its application, Neural Comput. Appl. 24 (2014) 125–132.
[39] M. Le Van Quyen, J. Foucher, J.-P. Lachaux, E. Rodriguez, A. Lutz, J. Martinerie, F.J. Varela, Comparison of Hilbert transform and wavelet methods for the analysis of neuronal synchrony, J. Neurosci. Methods 111 (2001) 83–98.
[40] J. Sun, M. Small, Unified framework for detecting phase synchronization in coupled time series, Phys. Rev. E 80 (2009) 046219.
[41] Y. Wang, B. Hong, X. Gao, S. Gao, Phase synchrony measurement in motor cortex for classifying single-trial EEG during motor imagery, in: Engineering in Medicine and Biology Society, 28th Annual International Conference of the IEEE, EMBS'06, 2006, pp. 75–78.
[42] R.T. Canolty, C.F. Cadieu, K. Koepsell, R.T. Knight, J.M. Carmena, Multivariate phase–amplitude cross-frequency coupling in neurophysiological signals, IEEE Trans. Biomed. Eng. 59 (2012) 8–11.
[43] S.R. Jammalamadaka, A. Sengupta, Topics in Circular Statistics, vol. 5, World Scientific, 2001.
[44] B. Schelter, M. Winterhalder, R. Dahlhaus, J. Kurths, J. Timmer, Partial phase synchronization for multivariate synchronizing systems, Phys. Rev. Lett. 96 (2006) 208103.
[45] S.H. Strogatz, From Kuramoto to Crawford: exploring the onset of synchronization in populations of coupled oscillators, Physica D, Nonlinear Phenom. 143 (2000) 1–20.
[46] P. Tass, M. Rosenblum, J. Weule, J. Kurths, A. Pikovsky, J. Volkmann, A. Schnitzler, H.-J. Freund, Detection of n:m phase locking from noisy data: application to magnetoencephalography, Phys. Rev. Lett. 81 (1998) 3291.
[47] M. Palus, Detecting phase synchronization in noisy systems, Phys. Lett. A 235 (1997) 341–351.
[48] B. Boashash, Time–Frequency Signal Analysis and Processing: A Comprehensive Reference, Academic Press, 2015.
[49] A.R. Kammerdiner, P.M. Pardalos, Analysis of multichannel EEG recordings based on generalized phase synchronization and cointegrated VAR, in: Computational Neuroscience, Springer, 2010, pp. 317–339.
[50] S. Johansen, Estimation and hypothesis testing of cointegration vectors in Gaussian vector autoregressive models, Econometrica, J. Econom. Soc. (1991) 1551–1580.

[51] M. Jalili, E. Barzegaran, M.G. Knyazeva, Synchronization of EEG: bivariate and multivariate measures, IEEE Trans. Neural Syst. Rehabil. Eng. 22 (2014) 212–221.
[52] J. Wackermann, Beyond mapping: estimating complexity of multichannel EEG recordings, Acta Neurobiol. Exp. 56 (1995) 197–208.
[53] J.G. Proakis, M. Salehi, Digital Communications, McGraw–Hill, 2008.
[54] M. Breakspear, S. Heitmann, A. Daffertshofer, Generative models of cortical oscillations: neurobiological implications of the Kuramoto model, Front. Human Neurosci. 4 (2010) 10.3389.
[55] D. Cumin, C. Unsworth, Generalising the Kuramoto model for the study of neuronal synchronisation in the brain, Physica D, Nonlinear Phenom. 226 (2007) 181–196.
[56] M. Khlif, P. Colditz, B. Boashash, Effective implementation of time–frequency matched filter with adapted pre and postprocessing for data-dependent detection of newborn seizures, Med. Eng. Phys. 35 (2013) 1762–1769.
[57] G.P. Nason, B.W. Silverman, The Stationary Wavelet Transform and Some Statistical Applications, Lecture Notes in Statistics, Springer Verlag, New York, 1995, p. 281.
[58] P. Zarjam, J. Epps, N.H. Lovell, Beyond subjective self-rating: EEG signal classification of cognitive workload, IEEE Trans. Auton. Ment. Dev. 7 (2015) 301–310.
[59] W.A. Truccolo, M. Ding, K.H. Knuth, R. Nakamura, S.L. Bressler, Trial-to-trial variability of cortical evoked responses: implications for the analysis of functional connectivity, Clin. Neurophysiol. 113 (2002) 206–226.
[60] M. Pedersen, A. Omidvarnia, E.K. Curwood, J.M. Walz, G. Rayner, G.D. Jackson, The dynamics of functional connectivity in neocortical focal epilepsy, NeuroImage, Clinical 15 (2017) 209–214.
[61] A. Omidvarnia, M. Pedersen, D.N. Vaughan, J.M. Walz, D.F. Abbott, A. Zalesky, G.D. Jackson, Dynamic coupling between fMRI local connectivity and interictal EEG in focal epilepsy: a wavelet analysis approach, Hum. Brain Mapp. 38 (2017) 5356–5374.
[62] J.M. Walz, M. Pedersen, A. Omidvarnia, M. Semmelroch, G.D. Jackson, Spatiotemporal mapping of epileptic spikes using simultaneous EEG-functional MRI, Brain 140 (2017) 998–1010.
[63] W. Jian, M. Chen, D.J. McFarland, Use of phase-locking value in sensorimotor rhythm-based brain–computer interface: zero-phase coupling and effects of spatial filters, Med. Biol. Eng. Comput. 55 (2017) 1915–1926.

Payam Shahsavari Baboukani received his B.Sc. and M.Sc. degrees in biomedical engineering from IAU and Razi University in 2014 and 2016, respectively. His areas of interests are EEG signal processing and pattern recognition.

Ghasem Azemi received his Ph.D. degree in Signal Processing from Queensland University of Technology, Brisbane, Australia in 2004. He then joined the Department of Electrical Engineering, Razi University, Kermanshah, Iran where he is now an Associate Professor. Between 2010 and 2014, he was with the Centre for Clinical Research, The University of Queensland, Brisbane, Australia as a Research Fellow. His research interests include biomedical and time–frequency signal processing.

Boualem Boashash is a Scholar, Professor, and Senior Academic with experience in five leading Universities in France and Australia, mostly at The University of Queensland (UQ) and QUT. He has published more than 500 technical publications, including more than 125 journal publications covering engineering, applied mathematics, and bio-medicine. He pioneered the field of time–frequency signal processing for which he published the most comprehensive book and most powerful software package. Among many initiatives, he founded ISSPA, a leading conference since 1985. On leave from UQ, he took an appointment in the UAE as the Dean of Engineering, then moved to Qatar University. Since 2017, he is back with UQ. In 2018, at the time of publication, his work had been cited over 15,000 times.

Paul Colditz is Professor of Perinatal Medicine at the University of Queensland, Australia with senior roles in research, teaching, clinical practice and professional management. As well as medical specialist qualifications in Australia and the UK (MBBS, FRACP, FRCPCH), he has a Master's degree in biomedical engineering and a PhD from the University of Oxford. His research focuses on clinically important perinatal health problems and translation to clinical practice and includes innovative research on brain injury and neuroprotection, seizure identification and treatment, neural plasticity and pathways to improving neurodevelopmental outcomes. He has a national and international profile in perinatal research particularly in the development of the preterm brain connectome and EEG. He has several high impact publications that define current clinical practice and has commercialization and entrepreneurial experience.

Amir Omidvarnia received his B.Sc. and M.Sc. degrees in 2002, 2005 from Amirkabir University of Technology and University of Tehran, and his Ph.D. from The University of Queensland in 2014, all in Biomedical Engineering. He is currently a senior researcher at Epilepsy Imaging division of the Florey Institute of Neuroscience and Mental Health, The University of Melbourne. His research interests are medical signal processing, brain functional connectivity analysis and multimodal neuroimaging.